scientific reports

Check for updates

OPEN

Enhanced adsorptive removal of ammonia nitrogen from wastewater by EDTA-2Na modified vermiculite

Jiabao Qu[1,2], Bingfei Yang[1,2,3]✉, Yan Li[1], Siyu Ma[1] & Yanjin Zheng[1,2,3]✉

Ammonia nitrogen (NH_3-N), a prevalent persistent and refractory pollutant in aqueous environments, compromises ecosystem structural integrity and poses potential risks to human health due to its long-term persistence. The development of efficient and cost-effective technologies for its removal is therefore imperative. In this study, a novel vermiculite-based adsorbent was fabricated through modification with ethylenediaminetetraacetic acid disodium salt (EDTA-2Na), designated as E-V. Compared to natural vermiculite (NV), the modified adsorbent exhibits a significant enhancement in ammonia nitrogen adsorption performance. Specifically, the 0.3E-V variant achieved an adsorption capacity of 18.45 mg·g^{-1} with a maximum removal efficiency of 95%, representing a 50% improvement over NV. The adsorption process was well-described by the pseudo-second-order kinetic model and the Freundlich isotherm model, suggesting that chemical and multilayer adsorption are the dominant mechanisms. Furthermore, application of the intraparticle diffusion model indicated that the adsorption process is co-governed by intraparticle diffusion and liquid film diffusion. These results provide valuable insights into the potential of natural vermiculite for wastewater treatment.

Keywords Ammonia nitrogen, Vermiculite, EDTA-2Na, Adsorption, Ion exchange

Ammonia nitrogen (NH_3-N) pollution is a ubiquitous inorganic pollutant in water bodies[1], characterized by extensive sources and large discharge volumes. Significant quantities of industrial wastewater, including those from oil refining wastewater, pharmaceutical wastewater, and food industry wastewater, as well as landfill leachate, contain high concentrations of NH_3-N, imposing continuous environmental pressure. Elevated NH_3-N concentrations trigger eutrophication and induce anoxic/anaerobic conditions in aquatic systems, thereby disrupting the ecosystem stability[2]. Moreover, dissolved ammonium (NH_4^+) can be converted to nitrite (NO_2^-) by nitrifying bacteria, posing substantial risks to drinking water safety[3]. Thus, developing a cost-effective and environmentally friendly approach for NH_3-N removal is of significant practical importance.

Conventional NH_3-N remediation technologies include biological processes[4,5], chemical precipitation[6,7], and adsorption[8,9]. Among these, adsorption has garnered widespread attention due to its operational simplicity, cost-effectiveness, high efficiency, and environmental benignity, making it a promising technology for practical applications[10]. Adsorption methods primarily utilize materials such as ion-exchange resins[11,12], metal-organic frameworks (MOFs)[13,14], and clay minerals. Compared to ion-exchange resins and MOFs, clay mineral-based adsorbents have emerged as ideal candidates owing to their favorable selective adsorption properties, ion-exchange capabilities, and alignment with sustainable development goals[15]. Studies have demonstrated that clay minerals, such as bentonite, zeolite and attapulgite, when subjected to thermal activation[16], alkalization[17], or salt modification[18], exhibit significantly enhanced NH_3-N removal capacity. Among these minerals, natural vermiculite (NV), a layered clay material, has been increasingly applied in wastewater purification due to its excellent cation-exchange capacity, adsorption performance, thermal expansibility, and cost-effectiveness.

NV and its modified derivatives have received considerable attention as adsorbents for wastewater treatment. Relevant studies have shown that NV exhibits significant adsorption capacity for heavy metal ions such as Cr(VI), Pb(II), and Cu(II) in aqueous solutions, and its adsorption performance can be further enhanced

[1]College of Gems and Materials, Hebei GEO University, Shijiazhuang 052161, China. [2]Engineering Research Center for Silicate Solid Waste Resource Utilization of Hebei Province, Shijiazhuang 052161, China. [3]Hebei Key Laboratory of Green Development of Rock and Mineral Materials, Shijiazhuang 052161, China. ✉email: u7758@126.com; 002912@hgu.edu.cn

through chemical modification[19–21]. In recent years, vermiculite-based materials have also been increasingly employed for NH_3-N adsorption. Dias et al.[22] demonstrated that vermiculite, after modification with sodium hydroxide (NaOH) and hydrochloric acid (HCl), undergoes cation exchange. Adsorption tests revealed that HCl modification led to the replacement of K^+ by Al^{3+}, whereas NaOH modification resulted in its replacement by Mg^{2+} and Na^+. For both modifiers, the optimal concentration was 0.1 mol·L^{-1}. Ferreira et al.[23] used expanded vermiculite to adsorb NH_3-N from landfill leachate. In bench-scale tests employing a fixed-bed column, two bed heights and three flow rates were evaluated, and these tests yielded an average uptake capacity of 33.4 mg·g^{-1} at an NH_3-N concentration of 2,560 mg·L^{-1}. In pilot-scale tests conducted with a single stainless-steel column, an average uptake capacity of 18.1 mg·g^{-1} was obtained with an initial NH_3-N concentration of 1,193 mg·L^{-1}. Ren et al.[24] developed a convenient method for removing high concentrations of NH_3–N from wastewater using NaCl-modified vermiculite. They prepared a series of modified vermiculite samples (Na–V) using NaCl solutions at varying concentrations. The NH_3–N adsorption performance of Na–V was significantly enhanced compared to that of natural vermiculite (NV). Among these, vermiculite modified with 180 g·L^{-1} NaCl yielded the highest ammonium adsorption capacity (Q_m) of 11.569 mg·g^{-1}, which was 63.43% higher than that of NV (Q_m = 7.079 mg·g^{-1}). Currently, most studies focus on modifying NV using different chemical modifiers to enhance its adsorption performance. However, such single modification methods rely relatively heavily on the inherent cation-exchange capacity of the matrix itself, which limits further improvement in the adsorption performance of NV-based adsorbents. Therefore, exploring a low-cost, environmentally friendly modification method that can efficiently enhance the adsorption capacity for NH_3-N removal from water is of great practical significance.

In this study, NV was used as the base matrix and modified with ethylenediaminetetraacetic acid disodium salt (EDTA-2Na) to improve the NH_3-N removal capacity. This approach leverages the strong complexing ability of EDTA for cations[25], and the ion exchange between its Na^+ and the Mg^{2+}, Al^{3+}, and Fe^{3+} in NV. The objective was to develop an efficient method for removing NH_3-N from water. To investigate the removal mechanism and performance of EDTA-2Na-modified vermiculite (E-V), the powder structures of NV and E-V were characterized. Their adsorption isotherms and kinetic characteristics were determined. Combined with static adsorption experiments, the effects of solution pH, E-V dosage, and common coexisting cations (K^+, Ca^{2+}, Mg^{2+}) on NH_3-N adsorption performance were systematically evaluated.

Materials and methods

Materials

NV was obtained from Hebei Province, China. Prior to use, the raw NV was subjected to pretreatment involving crushing, purification, and grinding. All chemical reagents used were of analytical grade. Ammonium chloride (NH_4Cl), ethylenediaminetetraacetic acid disodium salt (EDTA-2Na), and potassium sodium tartrate ($NaKC_4H_4O_6$) were purchased from Sinopharm Chemical Reagent Co., Ltd. (Shanghai, China). Hydrochloric acid (HCl) and sodium hydroxide (NaOH) were procured from XiLong Science Co., Ltd. (Guangzhou, China). Deionized water was used throughout the experiments. Simulated NH_3-N wastewater was prepared by dissolving an appropriate amount of NH_4Cl in deionized water.

Modification of NV

The NV samples were ground in a mortar, sieved through a 200-mesh sieve, and stored for subsequent use. EDTA-2Na solutions with concentrations of 0.1, 0.2, and 0.3 mol·L^{-1} were prepared in beakers. As schematically illustrated in Fig. 1, the NV was added to the EDTA-2Na solutions at a solid-to-liquid ratio of 1:30 (g: mL). The mixtures were transferred to a constant-temperature magnetic stirrer for continuous agitation at 160 rpm for 12 h. Subsequently, solid-liquid separation was conducted, and the solid residues were thoroughly rinsed with deionized water to remove any unreacted EDTA-2Na. The washed solids were dried in an oven at 105 °C for 2 h, followed by regrinding and sieving through a 200-mesh sieve. This procedure yielded three modified vermiculite samples: 0.1E-V, 0.2E-V, and 0.3E-V, corresponding to modifications with 0.1, 0.2, and 0.3 mol·L^{-1} EDTA-2Na, respectively.

Material characterization

The surface morphology and microzone composition of the materials were characterized by scanning electron microscopy with energy-dispersive X-ray spectroscopy (SEM-EDS, ZEISS-Sigma300, Germany). The crystal structure, phase composition, and lattice parameters were analyzed using an X-ray diffractometer (XRD, Rigaku-SmartLab 9KW, Japan). The chemical structures, functional groups, and molecular vibrations were identified by Fourier-transform infrared spectroscopy (FT-IR, Thermo Fisher-Nicolet iS 5, USA). The specific surface area and pore volume distribution of the samples were determined from nitrogen adsorption-desorption experiments performed on a surface area analyzer (Micromeritics-ASAP 2420, USA). The specific surface area was calculated using the multi-point Brunauer-Emmett-Teller (BET) method, and the total pore volume was evaluated by the Barrett-Joyner-Halenda (BJH) method. The zeta potential of 0.E-V was analyzed using a zeta potential analyzer (Model: Zetasizer Nano ZS90, Brookhaven Instruments Corporation, USA).

Static adsorption experiments

Equal masses of 0.1E-V, 0.2E-V, and 0.3E-V adsorbents were added to separate 50 mL aliquots of simulated NH_3-N wastewater, each with an identical initial concentration. The pH of each system was adjusted to 7.0 using 0.1 mol·L^{-1} HCl or NaOH solutions. The mixtures were then agitated on a constant-temperature magnetic stirrer at 25 °C and 160 rpm for 2 h. Upon completion of the adsorption process, solid-liquid separation was achieved by centrifugation at 5000 rpm for 5 min. The residual NH_3-N concentration in the supernatant was determined spectrophotometrically using Nessler's reagent. All experiments were conducted in triplicate, and the results are

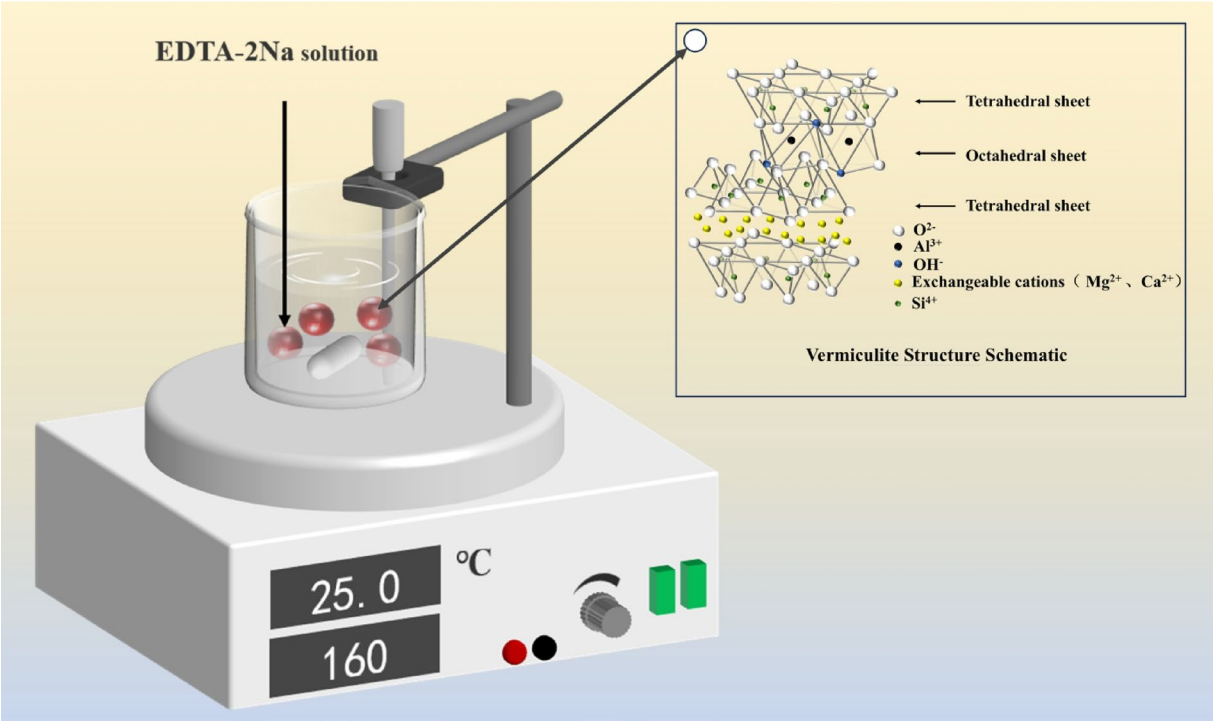

Fig. 1. Preparation steps of the E-V adsorbent.

expressed as mean values. Based on these results, the 0.3E-V sample, which demonstrated the highest NH_3-N removal efficiency, was selected for all subsequent experiments.

Effect of adsorbent dosage
The dosage of 0.3E-V was varied from 0 to 20 g·L^{-1}, while the initial NH_3-N concentration was maintained at 10 mg·L^{-1} and the solution pH was maintained at 7. The mixtures were then agitated at 25 °C and 160 rpm for 4 h. Subsequently, the samples were centrifuged, filtered, and analyzed to determine the residual NH_3-N concentration.

Effect of solution pH
The initial pH of the simulated wastewater was adjusted to values ranging from 3 to 10 using 0.1 mol·L^{-1} HCl or NaOH, while the dosage of 0.3E-V and the initial NH_3-N concentration were fixed at 10 g·L^{-1} and 10 mg·L^{-1}, respectively. The adsorption experiments were conducted under identical stirring and separation conditions to those previously described.

Effect of coexisting cations
Simulated wastewater containing 10 mg·L^{-1} NH_3-N and different concentrations of K^+, Ca^{2+} and Mg^{2+} (2, 5, 10 mmol·L^{-1}), introduced as KCl, $CaCl_2$ or $MgCl_2$, was prepared. The dosage of 0.3E-V and the solution pH were maintained constant at 10 g·L^{-1} and 7, respectively. The adsorption and analysis procedures were identical to those mentioned earlier.

Isothermal adsorption experiments

The initial pH of the solution was adjusted to 7, and the dosage of 0.3E-V was fixed at 10 g·L^{-1}. The initial NH_3-N concentration was varied from 0 to 40 mg·L^{-1}. The mixtures were agitated at 25 °C and 160 rpm for 4 h to ensure adsorption equilibrium was reached. After the adsorption process, the mixtures were centrifuged at 5000 rpm for 5 min, and the supernatants were filtered through a 0.45 μm membrane filter. The equilibrium NH_3-N concentration in the filtrate was determined, and the corresponding equilibrium adsorption capacity (Q_e) was calculated. All experiments were conducted in triplicate, and average values were used for data fitting.

Adsorption kinetics experiments

The initial NH_3-N concentration (10 mg·L^{-1}), solution pH (7), and 0.3E-V dosage (10 g·L^{-1}) were kept constant. The mixtures were stirred at 25 °C and 160 rpm, and samples were collected at predetermined time intervals (0–500 min). The collected samples were centrifuged, and the supernatants were filtered through a 0.45 μm membrane for the determination of residual NH_3-N concentration. The adsorption capacity at each time interval (Q_t) was calculated, and kinetic models were employed to fit the experimental data. All experiments were performed in triplicate.

Equations used

- Calculate removal rate percentage (R):

$$R = \frac{(C_0 - C_e)}{C_0} \times 100\% \tag{1}$$

where C_0 and C_e are the initial and equilibrium concentrations of NH_4^+ ($mg \cdot L^{-1}$).

- Calculate the adsorbed amount of NH_4^+ (Q_e, $mg \cdot g^{-1}$):

$$Q_e = \frac{(C_0 - C_e)\, V}{m} \tag{2}$$

where V is the volume of solution (L), and m is the mass of the adsorbent (g).

- Langmuir model:

$$\frac{C_e}{Q_e} = \frac{C_e}{Q_m} + \frac{1}{Q_m \cdot K_L} \tag{3}$$

where Q_m is the theoretical maximum adsorption capacity ($mg \cdot g^{-1}$), and K_L is the Langmuir constant ($L \cdot mg^{-1}$).

- Freundlich model:

$$\ln Q_e = \ln K_F + \frac{1}{n} \ln C_e \tag{4}$$

where K_F is the Freundlich constant [$(mg \cdot g^{-1}) \cdot (L \cdot mg^{-1})^{1/n}$], and n is a constant indicative of adsorption intensity.

- Separation factor:

$$R_L = \frac{1}{1 + K_L C_0} \tag{5}$$

where R_L is the separation factor for the Langmuir isotherm.

- Pseudo-first-order model:

$$\ln (Q_t - Q_e) = \ln Q_e - K_1 t \tag{6}$$

where Q_t is the amount of ammonium adsorbed at time t ($mg \cdot g^{-1}$), Q_e is the amount adsorbed at equilibrium time ($mg \cdot g^{-1}$), and K_1 is the pseudo-first order (PFO) rate coefficient (min^{-1}).

- Pseudo-second-order model:

$$\frac{t}{Q_t} = \frac{1}{Q_e^2 K_2} + \frac{t}{Q_e} \tag{7}$$

where Q_t is the amount of ammonium adsorbed at time t ($mg \cdot g^{-1}$), Qe is the amount adsorbed at equilibrium ($mg \cdot g^{-1}$), and K_2 is the pseudo-second-order (PSO) rate coefficient ($g \cdot mg^{-1} \cdot min^{-1}$).

- Intra-particle diffusion model:

$$Q_t = K_d t^{1/2} + C \tag{8}$$

where K_d is the rate constant for intraparticle diffusion ($mg \cdot g^{-1} \cdot min^{-1/2}$), and C is a constant related to the boundary layer thickness ($mg \cdot g^{-1}$).

Results and discussion

Material characterization

SEM-EDS analysis

Figure 2 presents the SEM images of NV, 0.3E-V (before adsorption), and 0.3E-V after NH_3-N adsorption (designated as 0.3E-V + NH_3-N). As shown in Fig. 2a, NV displays a characteristic irregular lamellar structure with a relatively smooth surface, which aligns with the morphology reported for similar materials in the literature[26]. Following modification with 0.3 $mol \cdot L^{-1}$ EDTA-2Na (Fig. 2b), the layered structure of the resulting 0.3E-V appears partially exfoliated, revealing a more developed porous architecture alongside a notable increase

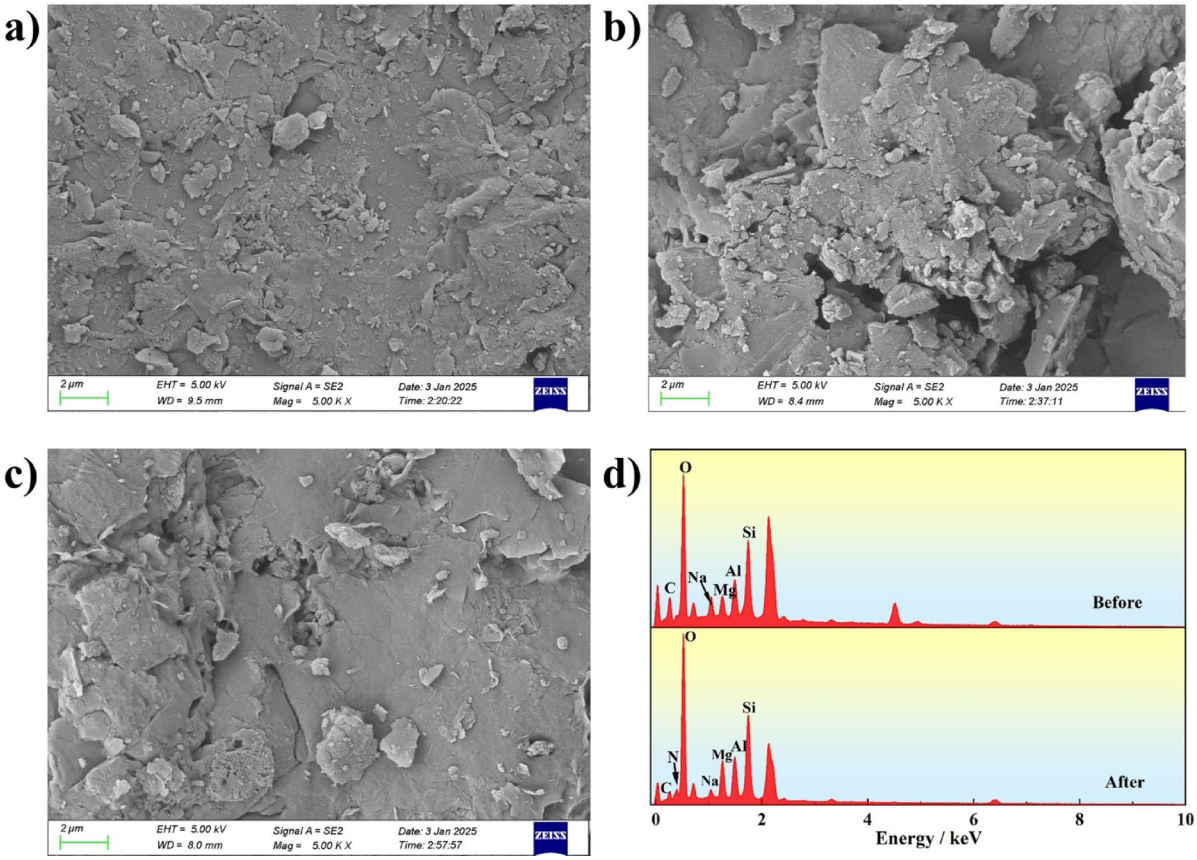

Fig. 2. (**a**) SEM image of NV, (**b**) SEM image of 0.3E-V, (**c**) SEM image of 0.3E-V after adsorption of NH_3-N, (**d**) EDS energy spectrum before and after adsorption of 0.3E-V.

Samples	wt%								
	Si	O	Al	Na	Mg	Fe	Ca	*N*	C
Pre-adsorption 0.3E-V	14.74	35.12	6.60	3.76	3.50	23.26	0.73	0.10	12.19
Post-adsorption 0.3E-V	14.03	34.66	7.24	1.70	3.29	25.68	0.64	2.10	10.66

Table 1. Changes in major elemental composition of 0.3E-V before and after adsorption.

in surface roughness[27]. These structural modifications are conducive to increasing the density of adsorption sites on the material surface, thereby creating favorable conditions for NH_3-N adsorption. Upon completion of the adsorption process (Fig. 2c), the surface of the 0.3E-V + NH_3-N exhibits significantly greater flatness compared to its state before adsorption. Complementary EDS elemental analysis (Table 1) shows that the mass fraction of nitrogen on the surface of 0.3E-V + NH_3-N reaches 2.16 wt%, which is 1.82 times higher than that of the pristine 0.3E-V. Concurrently, the mass fraction of sodium decreases from 3.76 wt% to 1.70 wt%. These characterization results collectively verify the successful loading of NH_3-N onto the 0.3E-V material.

XRD analysis

Figure 3 shows the XRD patterns of NV, 0.3E-V, and 0.3E-V + NH_3-N. The diffraction pattern of NV is dominated by peaks corresponding to quartz (SiO_2, PDF#46-1045) and vermiculite [$(Mg, Fe, Al)_3(Al, Si)_4O_{10}(OH)_2{\cdot}4H_2O$, PDF#16–0613]. This phase composition is consistent with literature reports for NV[28]. Compared to NV, the 0.3E-V sample shows a significant reduction in the intensity of the characteristic vermiculite peaks and the emergence of a new diffraction peak. This new peak, referred to herein as the V-P peak, is indicative of a vermiculite-phlogopite interstratified mineral structure[24]. Its appearance signifies a notable modification of the NV interlayer structure, which we attribute to structural collapse following the incorporation of alkaline cations (Na^+, K^+, Rb^+, Cs^+)[29]. The treatment with EDTA-2Na facilitates the chelation of EDTA anions with interlayer cations (Mg^{2+}, Ca^{2+})[25], which accelerates the ion exchange of Na^+ for the original interlayer cations and reduces the stability of the layered structure. Following NH_3-N adsorption, the intensity of the V-P diffraction peak in the NH_3-N-laden sample decreases relative to that in 0.3E-V. This observation is likely a consequence of the ion

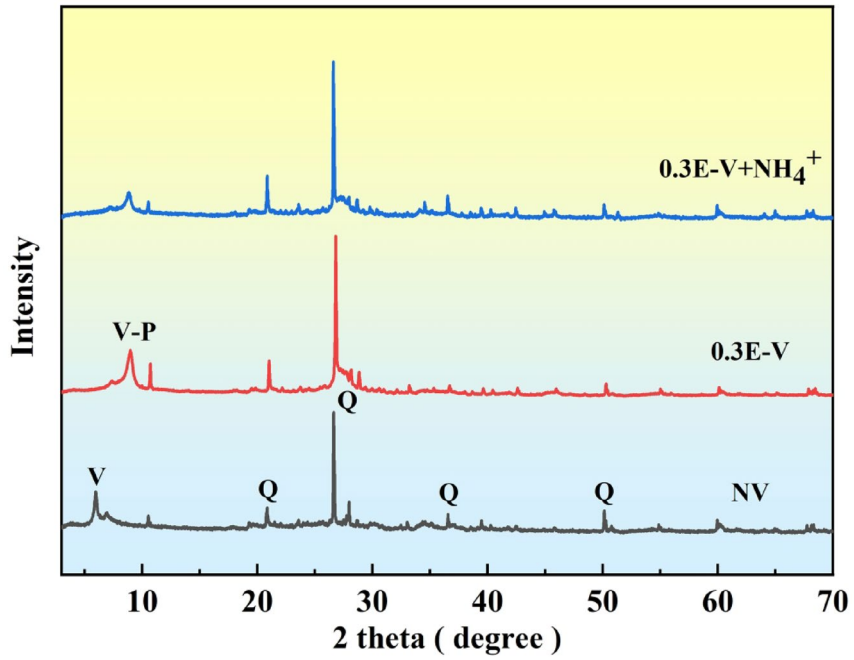

Fig. 3. XRD spectra of NV, 0.3E-V and 0.3E-V + NH_3-N (V - Vermiculite; V-P - vermiculite-phlogopite interlayer mineral structure; Q - Quartz).

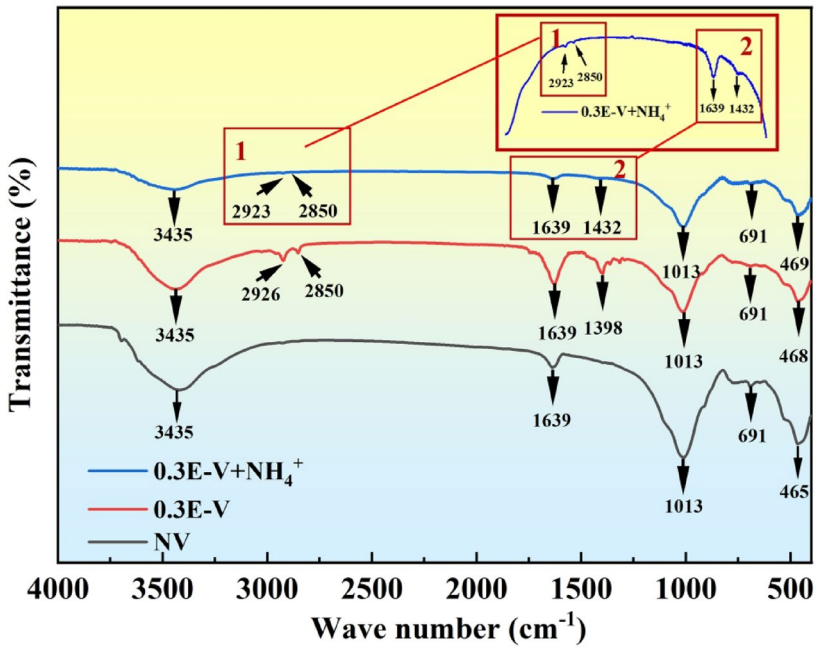

Fig. 4. FT-IR patterns of NV, 0.3E-V, 0.3E-V + NH_3-N.

exchange between NH_4^+ and the intercalated Na^+, leading to a further structural alteration that diminishes the characteristic V-P peak intensity[30].

FT-IR analysis

Figure 4 displays the FT-IR spectra of NV, 0.3E-V, and 0.3E-V + NH_3-N. All samples exhibit characteristic bands at 3435 cm^{-1} and 1639 cm^{-1}, corresponding to O-H stretching and bending vibrations of adsorbed water[31,32]. The strong peak at 1013 cm^{-1} along with those at 691 cm^{-1} and 465 cm^{-1} are assigned to Si-O, Al-O, and Si-O-Si vibrations, confirming the vermiculite structure[33]. In 0.3E-V, the notable weakening of peaks at 691 cm^{-1} and

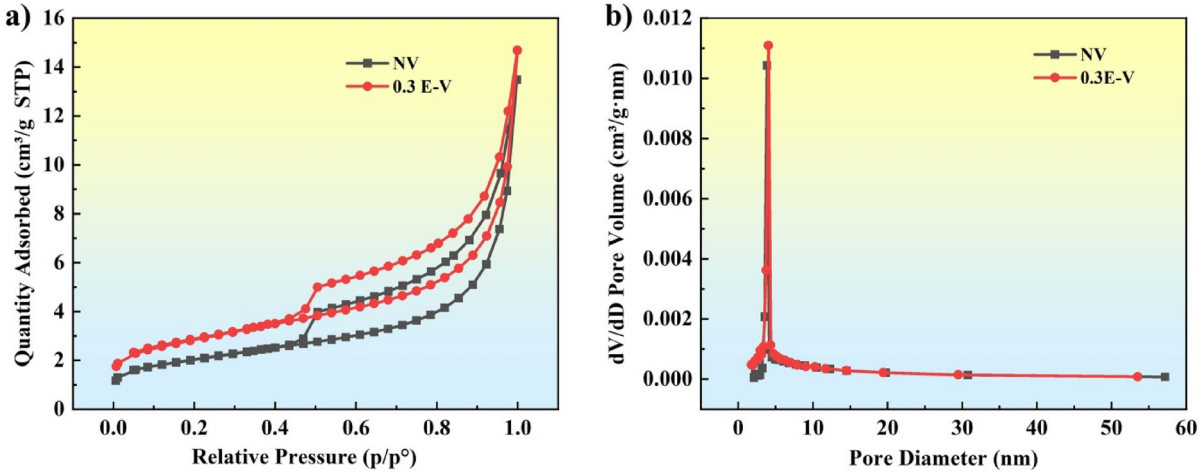

Fig. 5. (**a**) N_2 adsorption-desorption isotherms and (**b**) pore size distribution of NV, 0.3E-V adsorbent materials.

Samples	Specific surface area (m^2/g)	Microporous area (m^2/g)	Total pore volume (cm^3/g)	Micropore volume (cm^3/g)	Average pore size (nm)
NV	7.0916	1.0273	0.020858	0.000502	11.7652
0.3E-V	9.7801	1.9168	0.022709	0.000958	9.2879

Table 2. BET data for NV, 0.3E-V.

465 cm^{-1} suggests structural disruption, while new peaks at 2926 cm^{-1}, 2850 cm^{-1}, and 1398 cm^{-1}, characteristic of -CH_3, -NH, and C = O groups, verify the successful anchoring of EDTA-2Na[34]. After NH_3-N adsorption, the appearance of an NH_4^+ peak at 1432 cm^{-1} and the decrease in water-related peak intensities indicate ion exchange between interlayer Na^+ and NH_4^+[35]. The smaller hydration radius and lower hydration energy of NH_4^+ promote dehydration, potentially resulting in interlayer collapse[36]. These spectral findings align well with SEM and XRD analyses.

BET analysis

Figure 5 presents the N_2 adsorption-desorption isotherms and pore size distributions of NV and 0.3E-V, with corresponding BET parameters summarized in Table 2. As shown in Fig. 5a, both materials exhibit typical type IV isotherms, characteristic of mesoporous structures. The gradual increase in adsorption capacity indicates the progression from monolayer to multilayer adsorption of N_2 molecules on the mesoporous surface[19]. A type H_3 hysteresis loop is observed, commencing at a relative pressure P/P_0 >0.4348, which suggests the prevalence of slit-like pores with irregular geometries within the 0.3E-V particles. The pore size distribution (Fig. 5b) further confirms the typical mesoporous nature for 0.3E-V, showing a concentration of pores within this size range.

As indicated in Table 2, 0.3E-V possesses a larger specific surface area (9.7801 $m^2 \cdot g^{-1}$ vs. 7.0916 $m^2 \cdot g^{-1}$, a greater total pore volume (2.2709×10^{-2} $cm^3 \cdot g^{-1}$ vs. 2.0858×10^{-2} $cm^3 \cdot g^{-1}$), and an increased micropore volume (9.58×10^{-4} $cm^3 \cdot g^{-1}$ vs. 5.02×10^{-4} $cm^3 \cdot g^{-1}$), compared with NV, while its average pore size decreases from 11.7652 nm to 9.2879 nm. These alterations are attributed to ion exchange between Na^+ and interlayer Mg^{2+}/Ca^{2+} during modification, which disrupts the interlayer structure of NV and generates numerous new micropores and mesopores[37]. This structural transformation consequently increases the volumes of mesopores and micropores while reducing the average pore size. The enhanced specific surface area and pore volume of 0.3E-V provide more adsorption sites, thereby facilitating NH_3-N adsorption. The observed variations in specific surface area and pore structure corroborate the conclusion of interlayer disruption derived from XRD analysis and are consistent with relevant studies on clay mineral adsorption[38,39].

Adsorption mechanism of NH_3-N

Based on multi-scale material characterization and experimental data, the modification mechanism of EDTA-2Na and the hierarchical adsorption mechanism for NH_3-N were elucidated. The process involves two key steps. First, EDTA anions selectively chelate and extract free Ca^{2+}/Mg^{2+} from the interlayer spaces of NV. This process not only exposes additional adsorption sites but also creates space for subsequent Na^+ intercalation, thereby significantly enhancing the ion exchange capacity of the material. Second, the introduced Na^+ ions promote the expansion and reorganization of the NV interlayer structure, leading to an increased volume of mesopores and micropores and a larger specific surface area. These structural modifications further augment the density of available adsorption sites. Furthermore, NH_4^+, owing to its smaller hydrated ionic radius and lower hydration energy compared to Na^+, is preferentially adsorbed and readily undergoes ion exchange with the intercalated

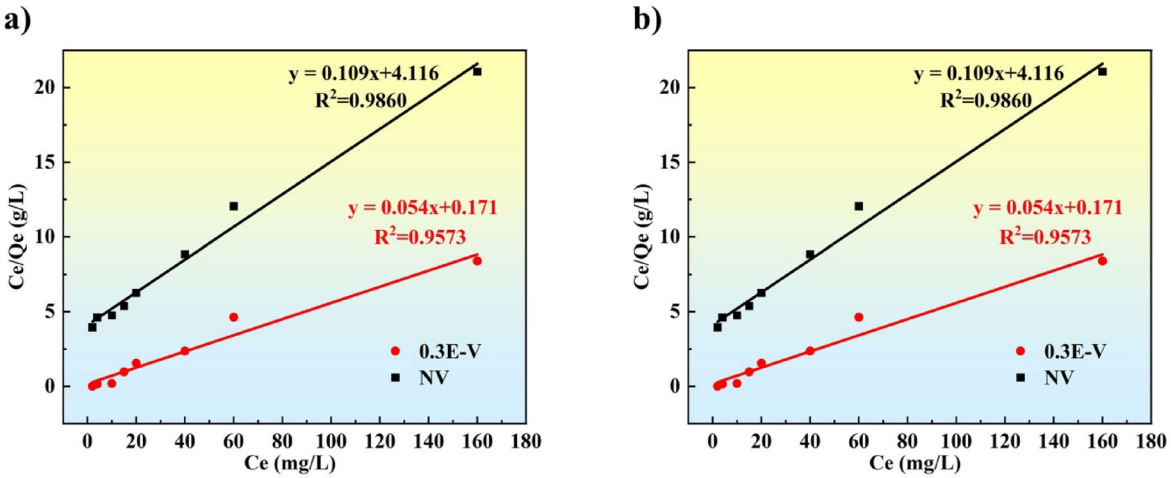

Fig. 6. Adsorption isotherms for NV, 0.3E-V: (**a**) Langmuir curve, (**b**) Freundlich curve.

Samples	Langmuir model			Freundlich model		
	Q_m	K_L	R_L^2	K_F	$1/n$	R_F^2
NV	9.15	0.0265	0.9860	0.056	0.8853	0.9952
0.3E-V	18.45	0.3138	0.9573	0.052	0.9228	0.9981

Table 3. Isothermal adsorption model fitting results.

Na^+. Collectively, these effects endow the 0.3E-V adsorbent with a greater specific surface area and more abundant adsorption sites, enabling a synergistic hierarchical adsorption process dominated by ion exchange and complemented by physical adsorption. This mechanism aligns with the adsorption characteristics of layered clay minerals and effectively overcomes the limited adsorption capacity of traditional adsorbents.

Adsorption isotherms and kinetics

Adsorption isotherms

The adsorption isotherms of NV and 0.3E-V were fitted using the Langmuir and Freundlich models, with results presented in Fig. 6; Table 3. For 0.3E-V, the Freundlich model provided a superior fit, as indicated by a higher coefficient of determination (R_F^2 = 0.9981). A Freundlich exponent ($1/n$ = 0.9228 < 1) indicates a thermodynamically favorable adsorption process. The proximity of the exponent to unity ($1/n \approx 1$) suggests a relatively homogeneous adsorbent surface, which also accounts for the reasonably good fit achieved with the Langmuir model. The theoretical maximum adsorption capacity derived from the Langmuir model was 18.45 $mg{\cdot}g^{-1}$, approximately twice that of NV (9.15 $mg{\cdot}g^{-1}$). Nevertheless, based on both the goodness-of-fit and the physical interpretation of the model parameters, the Freundlich model offers a more accurate description of the adsorption mechanism within the studied concentration range. This identifies the process as multilayer adsorption on a heterogeneous surface, which is consistent with a mechanism dominated by ion exchange[40].

Adsorption kinetics

The adsorption kinetics of NH_3-N onto 0.3E-V, as shown in Fig. 7a, exhibited a rapid initial phase within the first 2 h, followed by a gradual deceleration until equilibrium was reached. This commonly observed pattern is attributed to the high initial NH_3-N concentration and abundant available sites on the adsorbent surface, which collectively drive fast adsorption. As the reaction proceeds, the diminishing concentration gradient and the progressive occupation of active sites jointly reduce the mass transfer driving force, leading to the observed slowdown and eventual equilibrium.

To further elucidate the rate-limiting steps, the intra-particle diffusion model was applied (Fig. 7b; Table 4). The adsorption process was found to comprise three consecutive stages. The first involves rapid diffusion of NH_4^+ to the external surface and initial site occupation. This is followed by diffusion into the internal pores, and finally a stage approaching equilibrium where the rate declines markedly due to enhanced electrostatic repulsion and mass transfer resistance. The multi-linear nature of the Q_t versus $t^{1/2}$ plot, where none of the fitted lines pass through the origin, indicates that the adsorption process is co-controlled by liquid film diffusion and intraparticle diffusion, rather than being dominated solely by the latter[41].

Further analysis using pseudo-first-order and pseudo-second-order kinetic models (Fig. 7c and d; Table 5) showed that the pseudo-second-order model provided a superior fit (R_s^2 = 0.9998). This suggests that chemisorption-related processes act as a rate-limiting step, consistent with the ion exchange-dominated mechanism proposed in this study and thereby offering additional mechanistic support.

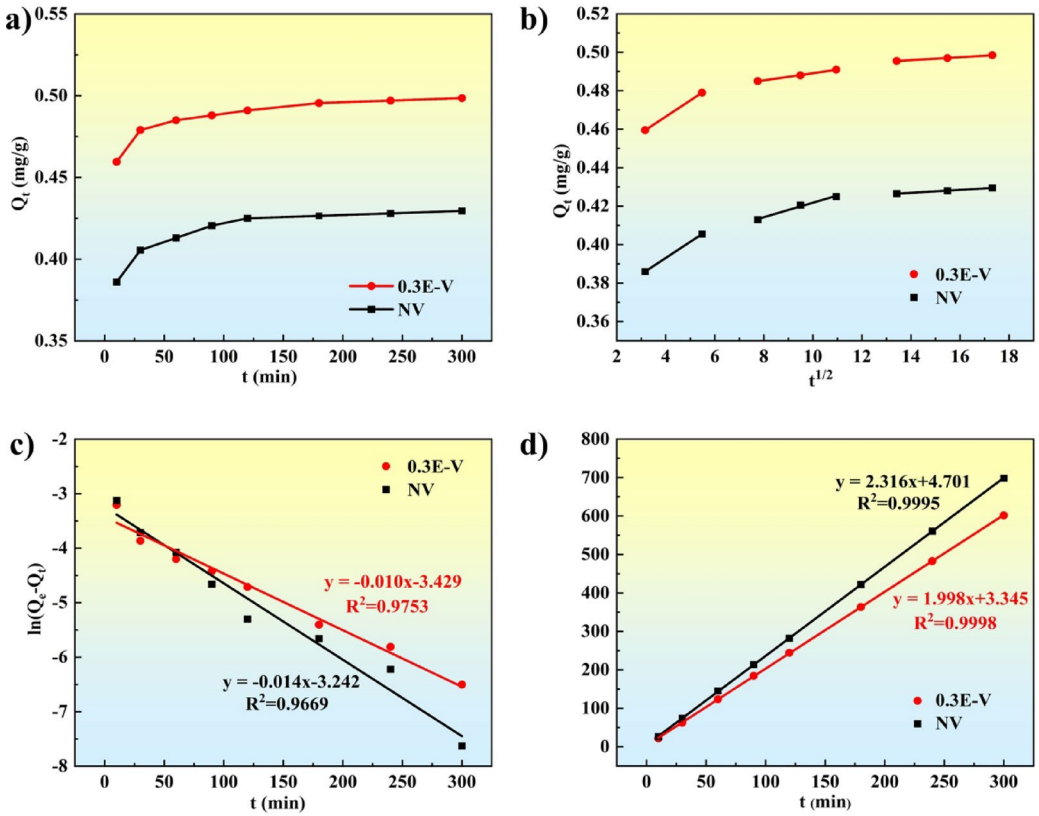

Fig. 7. (**a**) Shows the effect of contact time on the adsorption capacity of vermiculite, (**b**) intra-particle diffusion model, (**c**) PFO model for adsorption of NH_3-N, (**d**) PSO model for adsorption of NH_3-N.

Samples	Internal diffusion models					
	K_{d1} (mg/h$^{1/2}$/g)	R^2	K_{d2} (mg/h$^{1/2}$/g)	R^2	K^{d3} (mg/h$^{1/2}$/g)	R^2
NV	0.00841	0.999	0.00377	0.991	7.683×10^{-4}	0.998
0.3E-V	0.00841	0.999	0.00187	0.995	7.683×10^{-4}	0.998

Table 4. NV, 0.3E-V internal diffusion models.

Samples	Pseudo-first-order model		Pseudo-second-order model	
	K_1	R_f^2	K_2	R_s^2
NV	0.0140	0.9669	1.141	0.9995
0.3E-V	0.0104	0.9753	1.193	0.9998

Table 5. Adsorption kinetics of NH_3-N by NV, 0.3E-V.

Factors influencing NH_3-N adsorption

Effect of adsorbent dosage

Figure 8 illustrates the influence of adsorbent dosage on both the NH_3-N removal efficiency and the unit adsorption capacity. Under consistent experimental conditions, as the dosage of 0.3E-V increased from 1 to 60 g·L^{-1}, the NH_3-N removal efficiency rose markedly from 66.79% to 97.09%. This enhancement can be attributed to the increased dosage providing a greater specific surface area and more active sites, thereby facilitating the adsorption process[42]. Notably, when the dosage reached 20 g·L^{-1}, the removal efficiency achieved 95.88%, representing efficient removal. A further increase in dosage from 20 to 60 g·L^{-1} resulted in a considerably diminished growth rate of the removal efficiency. Concurrently, the unit mass adsorption capacity exhibited a continuous decline with increasing dosage. This trend is primarily due to the overlapping of active sites between

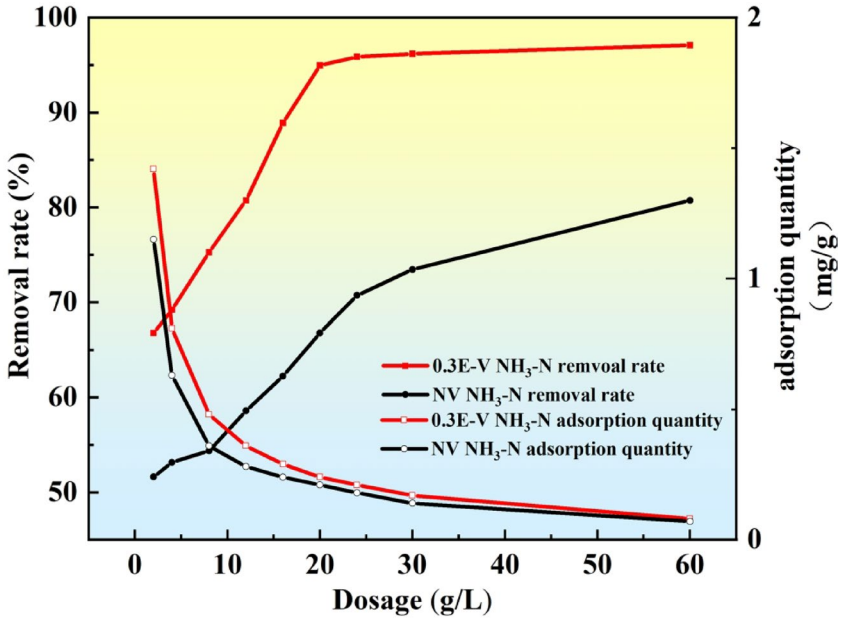

Fig. 8. Effect of dosage on the performance of adsorbed NH_3-N.

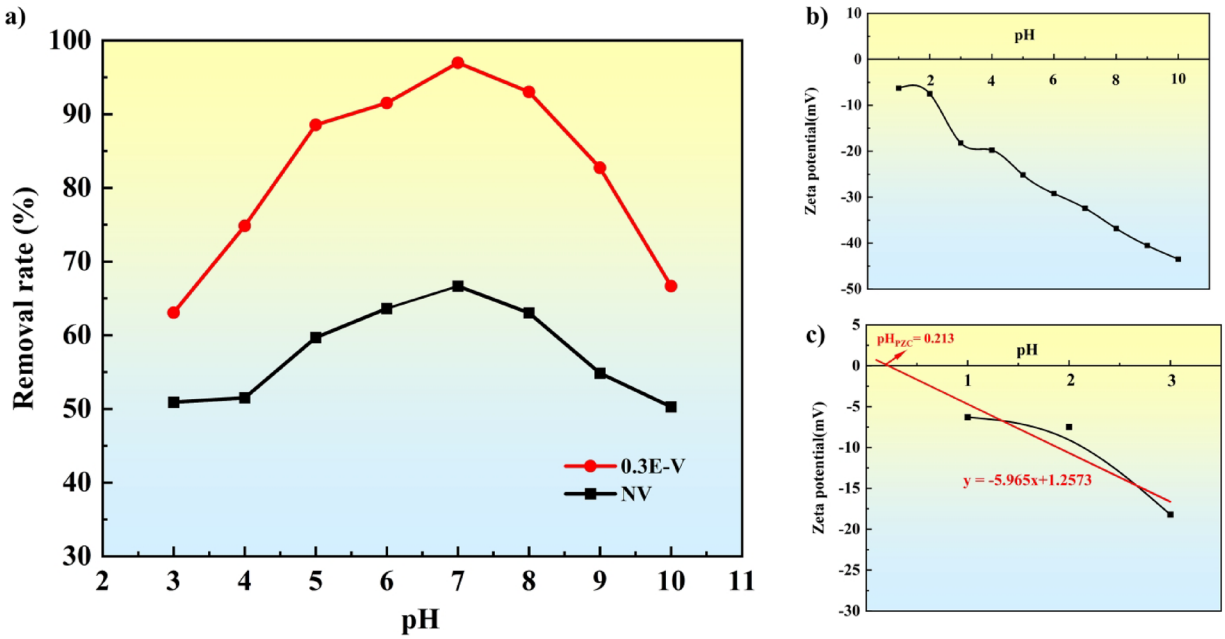

Fig. 9. (**a**) Effect of pH on the performance of adsorbed NH_3-N, (**b**) The potential values of 0.3E-V samples under different pH conditions and (**c**) The isoelectric point of 0.3E-V samples.

adsorbent particles. An excessive dosage leads to a surplus of adsorption sites in the system, which not only reduces site utilization efficiency but also represents an inefficient consumption of adsorbent material.

Effect of initial solution pH

The influence of the initial solution pH, ranging from 3 to 10, on the NH_3-N adsorption performance of NV and 0.3E-V was systematically investigated at the optimal adsorbent dosage of 20 $g{\cdot}L^{-1}$. As shown in Fig. 9a, 0.3E-V exhibited superior NH_3-N adsorption capacity and removal efficiency compared to NV across the entire pH range studied, confirming the effectiveness of the EDTA-2Na modification. The maximum NH_3-N removal efficiency of 0.3E-V reached 95.88% at pH 7, representing a 32.7% increase over the removal efficiency of 63.18% achieved by NV.

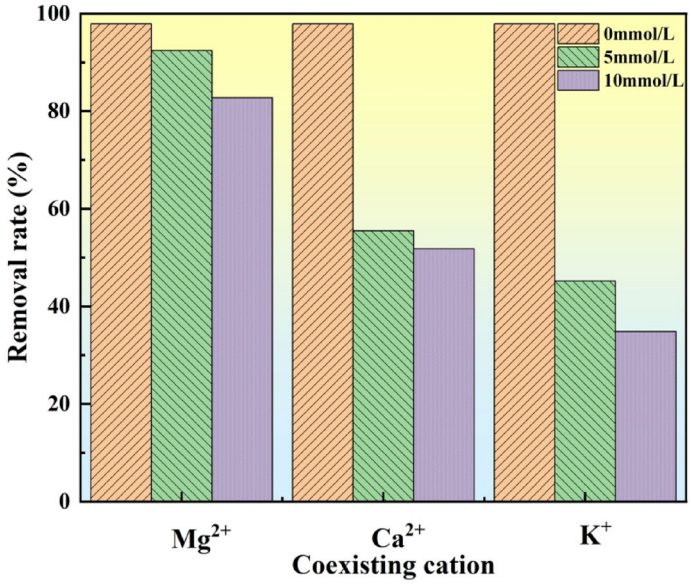

Fig. 10. Effect of co-existing ions on the adsorption performance of NH_3-N.

Zeta potential measurements (Fig. 9b) revealed that the surface charge of 0.3E-V remained negative throughout the studied pH range. This persistent negativity stems from the dissociation of carboxyl groups in EDTA, which impart a high density of negative charges onto the vermiculite surface, providing direct electrochemical evidence of successful modification[43].

The zeta potential data measured at pH 1, 2, and 3 were selected for fitting analysis[44], with the results shown in Fig. 9c. The pH value at which the zeta potential is zero is defined as the point of zero charge (pH_{PZC}); the pH_{PZC} of 0.3E-V was determined from the fitting curve to be 0.213. This low pH_{PZC} underscores the strong dependence of the adsorption mechanism on solution acidity. In acidic media, the high concentration of H^+ competes with NH_4^+ for active sites, with the higher adsorption energy of H^+ (-41.2 kJ·mol^{-1}) compared to NH_4^+ (-28.7 kJ·mol^{-1}) significantly inhibiting NH_3-N adsorption[45]. Under alkaline conditions, the rise in pH promotes the conversion of NH_4^+ to $NH_3{\cdot}H_2O$, while metal ions on the adsorbent surface react with OH^- to form hydroxide colloidal layers, collectively further hindering NH_3-N adsorption.

Effect of coexisting cations

Common cations in natural water bodies (K^+, Ca^{2+}, Mg^{2+}) may compete with NH_4^+ for adsorption sites, influencing NH_3-N removal efficiency. As illustrated in Fig. 10, the adsorption of NH_3-N by 0.3E-V was inhibited in a concentration-dependent manner with increasing levels of coexisting cations (2, 5, 10 mmol·L^{-1}), and the inhibition strength followed the order: $K^+ > Ca^{2+} > Mg^{2+}$. This phenomenon is primarily governed by the hydration radius effect: the hydration radii of Mg^{2+} (4.28 Å) and Ca^{2+} (4.12 Å) are larger than that of NH_4^+ (3.31 Å), whereas K^+ shares an identical hydration radius (3.31 Å) with NH_4^+, rendering K^+ more likely to occupy the same adsorption sites as NH_4^+[46]. Additionally, although divalent cations (Ca^{2+}, Mg^{2+}) exhibit stronger electrostatic affinity, their high hydration energies (Ca^{2+}: 1577 kJ·mol^{-1}; Mg^{2+}: 1921 kJ·mol^{-1}) restrict their migration to the solid-liquid interface, resulting in a relatively weaker competitive inhibition effect compared to K^+.

Conclusions

1. Vermiculite was modified with EDTA-2Na at varying concentrations (0.1–0.3 mol·L^{-1}), with the 0.3 mol·L^{-1} variant (0.3E-V) identified as optimal. Under conditions of pH 7 and a dosage of 20 g·L^{-1}, 0.3E-V achieved a maximum NH_3-N removal efficiency of 95.88%.
2. Competitive cation experiments revealed that K^+, Ca^{2+}, and Mg^{2+} all inhibit NH_4^+ adsorption, with K^+ showing the strongest effect due to its identical hydration radius to NH_4^+ (3.31 Å).
3. Adsorption isotherm analysis indicated that the Freundlich model (R_F^2 = 0.9981) better described the process, with a Freundlich exponent $1/n$ = 0.9228 (< 1) confirming favorable adsorption on a heterogeneous surface. Although the near-unity 1/n value allowed the Langmuir model (R_L^2 = 0.9573) to also provide a reasonable fit, the Freundlich model was deemed more representative across the studied concentration range, suggesting multilayer adsorption behavior. The theoretical maximum adsorption capacity of 0.3E-V was 18.45 mg·g^{-1}, 2.02 times that of natural vermiculite (9.15 mg·g^{-1}).
4. Kinetic studies showed that adsorption followed the pseudo-second-order model (R_s^2 = 0.9998, k_2 = 1.193 × 10^{-3} g·mg^{-1}·min^{-1}), indicating chemisorption as the rate-controlling step. The process was char-

acterized by an initial rapid phase dominated by surface adsorption, followed by a diffusion-controlled approach to equilibrium.

5. These results collectively support a synergistic adsorption mechanism for NH_3-N onto EDTA-2Na-modified vermiculite, dominated by ion exchange and complemented by physical adsorption.

Data availability

All data generated or analyzed are within the manuscript.

Received: 30 September 2025; Accepted: 27 November 2025
Published online: 07 December 2025

References

1. Yang, X. et al. Fast start-up of partial nitrification for high-ammonia wastewater treatment using zeolite with in-situ bioregeneration. *J. Water Process. Eng.* **59**, 105077. https://doi.org/10.1016/j.jwpe.2024.105077 (2024).
2. Wu, D., Yan, H., Shang, M., Shan, K. & Wang, G. Water eutrophication evaluation based on semi-supervised classification: A case study in three Gorges reservoir. *Ecol. Ind.* **81**, 362–372. https://doi.org/10.1016/j.ecolind.2017.06.004 (2017).
3. Wang, M. et al. Coupling Diazotization with oxidase-mimetic catalysis to realize dual-mode double-ratiometric colorimetric and electrochemical sensing of nitrite. *Sens. Actuators B-Chemical.* **355**, 131308. https://doi.org/10.1016/j.snb.2021.131308 (2022).
4. Li, P., Liu, M. H., Zhou, J. X., Chen, L. & Cai, M. F. Adsorption performance of different wetland substrates for ammonia nitrogen: an experimental study. *Water* **16**, 174. https://doi.org/10.3390/w16010174 (2024).
5. Gai, H. et al. An alternative scheme of biological removal of ammonia nitrogen from wastewater–highly dispersed Ru cluster @ mesoporous TiO_2 for the catalytic wet air oxidation of low-concentration ammonia. *Chem. Eng. J.* **407**, 127082. https://doi.org/10.1016/j.cej.2020.127082 (2021).
6. Huang, H., Liu, J., Zhang, P., Zhang, D. & Gao, F. Investigation on the simultaneous removal of fluoride, ammonia nitrogen and phosphate from semiconductor wastewater using chemical precipitation. *Chem. Eng. J.* **307**, 696–706 (2017).
7. Li, J. et al. Microbial induced calcium precipitation by Zobellella denitrificans sp. LX16 to simultaneously remove ammonia nitrogen, calcium, and chemical oxygen demand in reverse osmosis concentrates. *Environ. Res.* **240**, 117484. https://doi.org/10.1016/j.envres.2023.117484 (2024).
8. Huang, Z. et al. Adsorption - Catalytic ozonation of ammonia nitrogen in drinking water by alkali-modified NaX zeolites. *J. Water Process. Eng.* **60**, 105243. https://doi.org/10.1016/j.jwpe.2024.105243 (2024).
9. Zhou, H. & Ou, L. Adsorption of ammonia nitrogen in wastewater by tailing loaded manganese oxide material. *Inorg. Chem. Commun.* **144**, 109886. https://doi.org/10.1016/j.inoche.2022.109886 (2022).
10. Zhang, X., Gu, J. & Liu, Y. Necessity of direct energy and ammonium recovery for carbon neutral municipal wastewater reclamation in an innovative anaerobic MBR-biochar adsorption-reverse osmosis process. *Water Res.* **211**, 118058. https://doi.org/10.1016/j.watres.2022.118058 (2022).
11. Tabassum, S. A combined treatment method of novel mass bio system and ion exchange for the removal of ammonia nitrogen from micro-polluted water bodies. *Chem. Eng. J.* **378**, 122217. https://doi.org/10.1016/j.cej.2019.122217 (2019).
12. Akalın, H. A., Hiçsönmez, Ü. & Yılmaz, H. J. J. o. t. T. C. S. S. A. C. Removal of cesium from aqueous solution by adsorption onto Sivas-Yildizeli (Turkiye) vermiculite: equilibrium, kinetic and thermodynamic studies. **5**, 85–116. https://doi.org/10.18596/jotcsa.317771 (2017).
13. Zhao, J., Ren, G. & Meng, X. Recent advances on MOFs for photocatalytic and electrocatalytic nitrogen reduction to produce ammonia. *Nano Energy*. **130**, 110109. https://doi.org/10.1016/j.nanoen.2024.110109 (2024).
14. Bashkova, S. & Bandosz, T. J. Effect of surface chemical and structural heterogeneity of copper-based MOF/graphite oxide composites on the adsorption of ammonia. *J. Colloid Interface Sci.* **417**, 109–114. https://doi.org/10.1016/j.jcis.2013.11.010 (2014).
15. Babel, S. & Kurniawan, T. A. Low-cost adsorbents for heavy metals uptake from contaminated water: a review. *J. Hazard. Mater.* **97**, 219–243. https://doi.org/10.1016/s0304-3894(02)00263-7 (2003).
16. Erdogan, B., Ergurhan, O. & Anter, A. Influence of acid activation on the NH_3-adsorption properties of a Turkish bentonite. *Clay Miner.* **56**, 178–184. https://doi.org/10.1180/clm.2021.31 (2021).
17. Khalifa, A. Z. et al. Advances in alkali-activation of clay minerals. *Cem. Concr. Res.* **132**, 106050. https://doi.org/10.1016/j.cemconres.2020.106050 (2020).
18. Mendel, N., Siretanu, I., Mugele, F. & Brilman, D. W. F. W. Biogas upgrading using Cation-Exchanged bentonite clay. *Ind. Eng. Chem. Res.* **62**, 17883–17892. https://doi.org/10.1021/acs.iecr.3c01635 (2023).
19. Salih, S. S. et al. Chitosan-vermiculite composite adsorbent: Preparation, characterization, and competitive adsorption of Cu(II) and Cd(II) ions. *J. Water Process. Eng.* **59**, 105044. https://doi.org/10.1016/j.jwpe.2024.105044 (2024).
20. Salih, S. S., Kadhom, M., Shihab, M. A. & Ghosh, T. K. Competitive adsorption of Pb(II) and phenol onto modified Chitosan/Vermiculite adsorbents. *J. Polym. Environ.* **30**, 4238–4251. https://doi.org/10.1007/s10924-022-02515-0 (2022).
21. Mao, S. et al. Adsorption and co-adsorption of Chlorophenols and Cr(VI) by functional organo-vermiculite: experiment and theoretical calculation. *Sep. Purif. Technol.* **277**, 119638. https://doi.org/10.1016/j.seppur.2021.119638 (2021).
22. Dias, N. C., Steiner, P. A. & Braga, M. C. B. Characterization and modification of a clay mineral used in adsorption tests. *J. Minerals Mater. Charact. Eng.* **03**, 277–288. https://doi.org/10.4236/jmmce.2015.34030 (2015).
23. Ferreira, P. A. S., Dias, N. C., Barquilha, C. E. R., Braga, S. M. & Braga, M. C. Scaling-up of the adsorption process of ammonia nitrogen onto expanded vermiculite using fixed-bed columns. *Environ. Technol.* **44**, 304–315. https://doi.org/10.1080/09593330.2021.1970818 (2023).
24. Ren, S., Huang, S. & Liu, B. Enhanced removal of ammonia nitrogen from rare Earth wastewater by NaCl modified vermiculite: performance and mechanism. *Chemosphere* **302**, 134742. https://doi.org/10.1016/j.chemosphere.2022.134742 (2022).
25. Zhang, K. et al. EDTA-based adsorbents for the removal of metal ions in wastewater. *Coord. Chem. Rev.* **434**, 213809. https://doi.org/10.1016/j.ccr.2021.213809 (2021).
26. Chen, M. et al. The role of Fe(III) in enhancement of interaction between Chitosan and vermiculite for synergistic co-removal of Cr(VI) and Cd(II). *Colloids Surf. a-Physicochemical Eng. Aspects*. **606**, 125356. https://doi.org/10.1016/j.colsurfa.2020.125356 (2020).
27. Gai, H. et al. An alternative scheme of biological removal of ammonia nitrogen from wastewater–highly dispersed Ru cluster@ mesoporous TiO_2 for the catalytic wet air oxidation of low-concentration ammonia. *Chem. Eng. J.* **407**, 127082 (2021).
28. Ma, L. et al. The structural change of vermiculite during dehydration processes: A real-time in-situ XRD method. *Appl. Clay Sci.* **183**, 105332. https://doi.org/10.1016/j.clay.2019.105332 (2019).
29. Wu, H. et al. Exploring the relationship between Th(IV) adsorption and the structure alteration of phlogopite. *Appl. Clay Sci.* **152**, 295–302. https://doi.org/10.1016/j.clay.2017.11.026 (2018).

30. Valdes, H., Alejandro, S. & Zaror, C. A. Natural zeolite reactivity towards ozone: the role of compensating cations. *J. Hazard. Mater.* **227**, 34–40. https://doi.org/10.1016/j.jhazmat.2012.04.067 (2012).
31. He, Y., Lin, H., Dong, Y., Liu, Q. & Wang, L. Simultaneous removal of ammonium and phosphate by alkaline-activated and lanthanum-impregnated zeolite. *Chemosphere* **164**, 387–395. https://doi.org/10.1016/j.chemosphere.2016.08.110 (2016).
32. Amaya, J. et al. Modulation of the acidity of a vermiculite and its potential use as a catalytic support. *J. Mater. Sci.* **55**, 6482–6501. https://doi.org/10.1007/s10853-020-04445-5 (2020).
33. Chen, X. T., Tong, D. S., Fang, Z., Gao, Z. P. & Yu, W. H. Acid leaching vermiculite: A Multi-Functional solid catalyst with a strongly electrostatic field and bronsted acid for depolymerization of cellulose in water. *Molecules* **27**, 3149. https://doi.org/10.3390/molecules27103149 (2022).
34. Zhang, H., Li, R. & Zhang, Z. A versatile EDTA and Chitosan bi-functionalized magnetic bamboo Biochar for simultaneous removal of Methyl orange and heavy metals from complex wastewater. *Environ. Pollut.* **293**, 118517. https://doi.org/10.1016/j.envpol.2021.118517 (2022).
35. Zazoua, A. et al. Evidence of ammonium ion-exchange properties of natural bentonite and application to ammonium detection. *Mater. Sci. Eng. C-Materials Biol. Appl.* **33**, 5084–5089. https://doi.org/10.1016/j.msec.2013.09.005 (2013).
36. Fu, H. et al. Ammonium removal using a calcined natural zeolite modified with sodium nitrate. *J. Hazard. Mater.* **393**, 122481 (2020).
37. Feudjio, F. D. S. et al. Tunable water vapor adsorption properties on ion exchange microporous zeolite Na-X derived from natural Kaolin. *Inorg. Chem. Commun.* **177**, 114379. https://doi.org/10.1016/j.inoche.2025.114379 (2025).
38. Kuldeyev, E. et al. Modifying natural zeolites to improve heavy metal adsorption. *Water* **15**, 2215. https://doi.org/10.3390/w15122215 (2023).
39. Acar, B. C. & Yuksekdag, Z. Investigation of chromium (III) adsorption on Acid-Treated bentonite evaluation of Kinetic/Thermodynamic data. *Water Air Soil. Pollution*. **234**, 716. https://doi.org/10.1007/s11270-023-06727-5 (2023).
40. He, Q., Chen, X., Gong, S., Huang, L. & Xiao, Y. Adsorption behaviors and mechanisms of lanthanum ions and exchanger cations at halloysite-solution interface: perspectives from electrical double layer model and spectral analyses. *J. Mol. Liq.* **411**, 125711. https://doi.org/10.1016/j.molliq.2024.125711 (2024).
41. Ofomaja, A. E. Intraparticle diffusion process for lead(II) biosorption onto Mansonia wood sawdust. *Bioresour. Technol.* **101**, 5868–5876. https://doi.org/10.1016/j.biortech.2010.03.033 (2010).
42. Sang, W. et al. Na@La-modified zeolite particles for simultaneous removal of ammonia nitrogen and phosphate from rejected water: performance and mechanism. *Water Sci. Technol.* **82**, 2975–2989. https://doi.org/10.2166/wst.2020.541 (2020).
43. Zhou, L. M. et al. Honeycomb-like macroporous crosslinked Chitosan assisted EDTA-intercalated Ca-Mg-Al layered hydrotalcite composite foams for efficient U(VI) biosorption. *Int. J. Biol. Macromol.* **279** https://doi.org/10.1016/j.ijbiomac.2024.135011 (2024).
44. de Lint, W. S. et al. Ion adsorption parameters determined from zeta potential and Titration data for a γ-alumina nanofiltration membrane. *Langmuir* **19**, 5861–5868 (2003).
45. Li, J. et al. Insight into the adsorption mechanisms of aqueous hexavalent chromium by EDTA intercalated layered double hydroxides: XRD, FTIR, XPS, and zeta potential studies. *New J. Chem.* **43**, 15915–15923. https://doi.org/10.1039/c9nj03479j (2019).
46. Tansel, B. Significance of thermodynamic and physical characteristics on permeation of ions during membrane separation: hydrated radius, hydration free energy and viscous effects. *Sep. Purif. Technol.* **86**, 119–126. https://doi.org/10.1016/j.seppur.2011.10.033 (2012).

Acknowledgements

The authors extend their gratitude to Ms. Mengmeng Wang from Shiyanjia Lab (www.shiyanjia.com) for providing invaluable assistance with the XRD analysis.

Author contributions

J. Q. performed the investigation, wrote the original draft, and curated data. B. Y. managed the project administration, provided resources, and acquired funding. Y. L. managed the project administration. Y. Z. reviewed and edited the manuscript. S. M. conducted the investigation. All authors reviewed the manuscript.

Funding

The authors gratefully acknowledge the financial support from the Central Government Guiding Local Science and Technology Development Fund Project (216Z4101G).

Declarations

Competing interests

The authors declare no competing interests.

Additional information

Correspondence and requests for materials should be addressed to B.Y. or Y.Z.